# Transfer-matrix method of circular polarization light in an axionic photonic insulator

Anny C. Araújo ⬤, Sérgio Azevedo ⬤, and Cláudio Furtado ⬤

*Department of Physics, Federal University of Paraíba, João Pessoa, Paraíba, 58051-970, Brazil*

André J. Chaves

*Semiconductor Materials and Nanotechnology Group and Physics Department,*
*Aeronautics Institute of Technology, DCTA, São José dos Campos, São Paulo, 12228-900, Brazil*

Carlos H. Costa

*LAREB, Federal University of Ceará, Russas, Ceará, 62900-000, Brazil*

Claudionor G. Bezerra ⬤[*]

*Department of Physics, Federal University of Rio Grande do Norte, Natal, Rio Grande do Norte, 59072-970, Brazil*

The photonic analog of an axioniclike system (or electronic topological insulator) is called an axionic photonic crystal. These materials are classified by three physical properties: permittivity $\epsilon$, permeability $\mu$, and the topological parameter $\theta$. As a particular case, crystals with periodic $\epsilon$ and $\mu$ are the so-called photonic crystals. In this paper, we employ a transfer-matrix treatment to study the propagation of light waves in an axionic photonic crystal composed of alternating building layers $A$ and $B$. We present numerical results for the photonic band structure as a function of the ratio between permittivities $R = \epsilon_B/\epsilon_A$, layer thicknesses $X = d_B/d_A$, and topological parameters $\delta = \pi^2(\theta_A - \theta_B)^2/\alpha^2$. Our numerical results reveal that the band-gap features (width, center position, upper and lower frequencies) depend on the three parameters $\epsilon$, $\mu$, and $\theta$, but with the dependence on $\theta$ being stronger. In particular, as far as the band-gap width is concerned, we find that $X$ and $R$ work against each other; that is, as $X$ increases, $R$ must decreases for a wide band-gap emergence and vice versa. More interesting, however, are the results for the topological parameter $\theta$. We show that the presence of $\theta$ produces a photonic band gap (PBG) which depends only on the $\delta$ term. The widening of this PBG is slightly asymmetrical and monotonic as a function of $\delta$. It was also found that $\delta$ has no influence on the center position of the PBG. Our results open possibilities for technological applications of axionic photonic crystals with regard to the controlling and confinement of the propagation of light.

## I. INTRODUCTION

Photonic crystals (PCs) are very interesting optical materials with periodic dielectric properties. The first concept of periodic optical structure was introduced in 1887 by Lord Rayleigh, who carried out experiments with several periodic dielectric layered cells, nowadays called Bragg's mirror, and showed that they had a photonic band gap (PBG) [1]. A century later, in 1987, Yablonovitch [2] and John [3] independently investigated these optical structures in more than one dimension, and both suggested that those structures are capable of guiding and confining the propagation of light. They are nowadays referred to as photonic crystals [4]. Since the work of Yablonovitch and John, PCs have become, both theoretically and experimentally, attractive objects of research. This interest is related to the appearance of PBGs in those structures [2,3,5].

A timely question that naturally arises is why is it so important to study PBG materials with any number of dimensions? The importance of studying these materials lies in the way in which electromagnetic (EM) waves propagate within the bulk, enabling the investigation of many optical properties. For example, certain light wavelengths are allowed to pass through the structure; that is, in these materials the propagation of light is forbidden in some frequencies and directions [6]. Therefore, one can manipulate the propagation of light within a frequency range, adjusting the geometric, dielectric, and magnetic parameters of the photonic crystal, among others, in a manner very similar to the way in which a lattice of atoms can give rise to allowed and forbidden electronic bands. Thus, the absence of EM waves within a PBG in some frequency ranges can lead to some unusual features, with many potential applications in photonic devices [7].

Researchers have started to study quantum topological systems and have discovered a new class of matter, so-called topological insulators (TIs) [8,9]. Along with the advances in that research area, new classes of TIs, such as crystalline topological insulators, axion insulators, higher-order

―――――――
[*]cbezerra@fisica.ufrn.br

topological insulators, topological semimetals, and topological superconductors, have emerged [10–13]. In general, TIs are materials that present band gaps, but their bands are topologically distinct from the bands of a conventional insulator. Those differences are connected to the emergence of nontrivial band gaps perceived for the first time in two-dimensional (2D) TIs, also known as 2D quantum spin Hall insulators [8,14]. Thus, electron propagation inside of a TI is not allowed, but the edge electrons can move freely as surface modes. Therefore, the surface of a TI is filled with exotic topologically protected edge states, which means that the energy transport on the edges is topologically protected and robust against structural perturbations and disorder. Many theoretical and experimental demonstrations of TIs have been reported for electronic (fermionic) systems [13,15,16]. From an experimental perspective, (Hg,Cd)Te and monolayer hexagonal Sn, Sb were characterized as 2D TIs, and $(Bi,Sb)_2(Se,Te)_3$, $(Bi,Sb)_2Te_2Se$, $Bi_{2-x}Sb_xTe_{3-y}Se_y$, $TlBi(S,Se,Te)_2$, $Pb(Bi,Sb)_2Te_4$, $GeBi_2Te_4$, and $PbBi_4Te_7$ were characterized as three-dimensional (3D) TIs [16]. All of these materials have attracted increasing fundamental and technological interest around the world because of their excellent properties and characteristics such as low power dissipation, spin-polarized electrons [17], and more [16,18–21].

In the context of TIs, there is the axion insulator [11,22]. Axions are pseudoscalar weakly interacting low-mass particles and electrically neutral. However, even without electrical charge they can interact in an unusual way with the electromagnetic field. They were postulated in 1977 by the physicists Peccei and Quinn in order to explain the absence of charge-parity violation in the strong interaction between quarks in high-energy physics [23]. Despite intensive research, axions have not yet been observed in nature. The connection between axions and TIs relies on the fact that a term of the form $\theta(\vec{B} \cdot \vec{E})$ may be added to the standard Maxwell's Lagrangian without modifying the familiar laws of electricity and magnetism. The $\theta$ term is known in particle physics as the axionic field, but in condensed matter $\theta(\vec{B} \cdot \vec{E})$ is a generic expression which comes from the magnetoelectric effect present in three-dimensional topological materials and is analogous to the action that describes the coupling of the photon and the axion. Therefore, it can be applied to magnetoelectric materials, for instance, $Cr_2O_3$ (with $\theta \ll \pi$) [24–26]. Systems with time-reversal symmetry present a quantized value of $\theta$, being 0 for trivial insulators and $\pi$ for topological insulators. However, for magnetically ordered phases the value of $\theta$ can be arbitrary [27].

As a matter of fact, a remarkable development in 3D TIs is the so-called topological magnetoelectric effect (TME), in which the crossed induction of magnetization and electric polarization is expected to occur when external electric and magnetic fields are applied. This effect appears in the axion electrodynamics, which is known to describe the unusual magnetoelectric properties of 3D TIs [28–31]. For those reasons, TME of the kind that appears in TIs has been called "axion electrodynamics" [32]. One can understand that, in the context of electrodynamics, the axions' behavior is analogous to the TIs' behavior. Therefore, axions naturally emerged in condensed-matter physics as the effective low-energy theory for TIs, where these materials can be composed of periodic

arrangements with electric permittivity $\epsilon$, magnetic permeability $\mu$, and topological parameter $\theta$ modulated along a given direction [33]. The electrodynamics of an axion can be found in Ref. [34].

At the beginning of this century, Haldane and Raghu first investigated the electromagnetic analog of the electronic TI, which is the so-called photonic topological insulator (PTI) [35–39]. In their works, they predicted that photonic crystals made of magneto-optical materials could have topologically nontrivial bands and therefore could host topologically protected light states that unidirectionally propagate along the edges, with no possibility of backscattering. As the band structure is viewed, these edge states appear as continuous bands crossing the photonic band gap. As a consequence, light is allowed to unidirectionally propagate on the surface without scattering [40], in a manner very similar to electrons on the surface of a 2D TI [18,41]. The discovery of topological photonic systems has transformed our view of electromagnetic propagation and opened several venues of basic and applied science exploration. It also led to the understanding that much of the physics associated with the quantum Hall effect was not fundamentally quantum, but rather a very general wave phenomenon [39]. From an experimental perspective, the 3D topological photonic insulator was experimentally realized using a composite material consisting of split-ring resonators with strong magnetoelectric coupling which behaves like a "weak" TI (i.e., with an even number of surface Dirac cones) or a stack of 2D quantum spin Hall insulators [18]. In addition, recent advances in topological 2D, 3D, and higher-order PTIs have been observed [42]. In general, the advantage of these materials for technology is that topological photonic systems promise a new generation of photonic devices and communication systems [18,43,44].

The study of the propagation of electromagnetic waves in layered media has been the object of research for decades, for example, in chiral and bi-isotropic media (see Ref. [45]). There is also the growing field of topological photonics [37], which uses topological invariants, such as the Chern number, to classify and study photonic crystals. One such TI is the one-dimensional (1D) stacking of alternating dielectrics, whose properties can be mapped in the Su-Schrieffer-Heeger model, which has two distinct topological phases characterized by the winding number being 0 or 1 [46]. The interface between topological photonic crystals with different topologically regions can sustain edge states in a way similar to how topological insulators have conductive surface states [38,47,48]. However, less attention has been paid to the propagation of electromagnetic waves in layered axionic crystals.

In this paper, we use the powerful transfer-matrix method (TMM) to study the propagation of circularly polarized light waves through one-dimensional multilayers composed of two axionic photonic crystals, $A$ and $B$, which are characterized by the magnetoelectric effect, whose properties are dictated by the topological parameter $\theta$, similar to what happens in axion electrodynamics. This method shows how the light waves interact with the interface between alternating $A$ and $B$ layers of a photonic crystal [49]. We present numerical results for the photonic band structures as a function of the ratio between permittivities $R = \epsilon_B/\epsilon_A$, layer thicknesses $X = d_B/d_A$, and topological parameters $\delta = \pi^2(\theta_A - \theta_B)^2/\alpha^2$. In addition, we
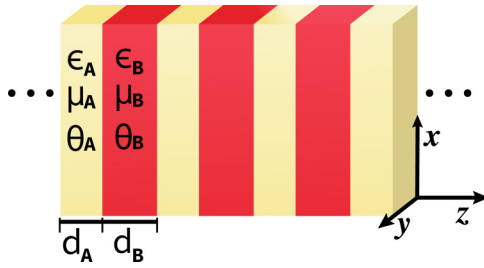
FIG. 1. Scheme of the 1D APC composed of alternating layers $A$ and $B$.

analyzed the width and frequencies of the center and lower and upper edges of the lowest band gap by varying $X$ and $R$ in photonic crystals, with different values of $\delta$, in order to map how the first band gap behaves as these parameters are changed. In this way, the propagation of light can be controlled through periodic modulation of the topological and lattice parameters, forming a band structure very similar to that of a conventional photonic crystal. This paper is organized as follows. In Sec. II we present the classical electromagnetic theory for a one-dimensional axionic photonic crystal (1D APC) made of two building blocks ($A$ and $B$), with their respective electric, magnetic, topological, and geometric parameters, which are periodically stacked along the $z$ direction. The transfer-matrix method for such a system, presenting the transmission (when the waves cross any interface) and propagation (when the waves propagate inside a given layer) matrices, is also described in Sec. II. In Sec. III we present our numerical results, which are the band structures of the one-dimensional APC, as a function of parameters $\delta$, $X$, and $R$, with emphasis on the behavior of the first gap. Finally, in Sec. IV we summarize the main results obtained in this work.

## II. PHYSICAL MODEL

We consider a 1D axionic photonic crystal composed of an arrangement of two layers, $A$ and $B$, with dielectric permittivities $\epsilon_A$ and $\epsilon_B$, magnetic permeabilities $\mu_A$ and $\mu_B$, topological parameters $\theta_A$ and $\theta_B$, and thicknesses $d_A$ and $d_B$, respectively, as described in Fig. 1. We choose a coordinate system such that the axionic photonic crystal is perpendicular to the $z$ axis. Throughout the entire paper we use SI units.

Here, we assume that the electrical permittivity $\epsilon(\vec{r})$, the magnetic permeability $\mu(\vec{r})$, and the topological angles $\theta(\vec{r})$ are real, isotropic, nondispersive, and periodic, with translation vector $\vec{R} = D\hat{z}$, where $D = d_A + d_B$ is the unit-cell size, i.e.,

$$\epsilon(\vec{r}) = \epsilon(\vec{r} + \vec{R}) \Rightarrow \epsilon(z) = \epsilon(z + D), \tag{1}$$

$$\mu(\vec{r}) = \mu(\vec{r} + \vec{R}) \Rightarrow \mu(z) = \mu(z + D), \tag{2}$$

and

$$\theta(\vec{r}) = \theta(\vec{r} + \vec{R}) \Rightarrow \theta(z) = \theta(z + D). \tag{3}$$

By using an analogy with classical axion electrodynamics, the modified constitutive relations, with the additional

topological term represented by $\theta$, are [30,34,50]

$$\vec{D} = \epsilon\vec{E} - \frac{\epsilon_0\alpha c\theta(\vec{r})}{\pi}\vec{B} \tag{4}$$

and

$$\vec{H} = \frac{\vec{B}}{\mu} + \frac{\alpha\theta(\vec{r})}{\mu_0 c\pi}\vec{E}. \tag{5}$$

Here, $\vec{E}$ and $\vec{D}$ are the electric and electric displacement fields, and $\vec{H}$ and $\vec{B}$ are the magnetic intensity and magnetic flux fields, respectively. In addition, $\alpha \approx 1/137$ is the fine-structure constant, $\theta$ is the dimensionless topological parameter, $c = 1/\sqrt{\mu_0\epsilon_0}$ is the light speed in vacuum, and $\epsilon_0$ and $\mu_0$ are the vacuum dielectric permittivity and magnetic permeability, respectively. In Eqs. (4) and (5), the dielectric permittivity $\epsilon$ and magnetic permeability $\mu$ are given by $\epsilon = \epsilon_0\epsilon_j$ and $\mu = \mu_0\mu_j$, where $\epsilon_j$ and $\mu_j$ ($j = A$ or $B$) are the relative dielectric permittivity and magnetic permeability, respectively, corresponding to layer $A$ or $B$. Another important point is that, in the classical context, the $\theta$ term can assume any value, and in general, this parameter characterizes the state of matter [32].

Maxwell's equations for a source-free and current-free system with monochromatic and oscillating fields, i.e., $\vec{E}, \vec{D}, \vec{H}, \vec{B} \propto e^{-i\omega t}$, can be written as

$$\vec{\nabla} \cdot \vec{D} = 0, \tag{6a}$$

$$\vec{\nabla} \cdot \vec{B} = 0, \tag{6b}$$

$$\vec{\nabla} \times \vec{E} = i\omega\vec{B}, \tag{6c}$$

$$\vec{\nabla} \times \vec{H} = -i\omega\vec{D}. \tag{6d}$$

Here, $\omega$ is the angular frequency. Notice that the magneto-electric features are introduced into the constitutive equations of the material and not directly into the Maxwell's equations [32].

### A. Transfer-matrix method

The TMM is a powerful approach for the analysis of light propagating through any multilayered media. Within the framework of the TMM, there are two kinds of matrices: (i) the transmission matrix, which connects the fields across an interface, and (ii) the propagation matrix, which describes the fields propagating inside a layer. In order to obtain both matrices we need to know how the electromagnetic waves behave at the boundaries.

In order to obtain the transfer matrix for the normal-incidence case, we start by considering the superposition of two different propagating waves with opposite directions on the $z$ axis and the same frequency. The boundary conditions that arise from the $\theta$ term imply that we need to consider the circularly polarized basis $\hat{v}_\lambda$, with $\lambda = + (-)$ labeling the right (left) rotation. After some algebra, we find that the total electric and magnetic fields in a medium $j$ ($= A, B$) are given by

$$\vec{E}_{j,\lambda} = [E_{j,\lambda}e^{ik_j z}\hat{v}_\lambda + E'_{j,\lambda}e^{-ik_j z}\hat{v}_\lambda] \tag{7}$$

and

$$\vec{H}_{j,\lambda} = [g_{j,\lambda}E_{j,\lambda}e^{ik_j z}\hat{v}_\lambda + \bar{g}_{j,\lambda}E'_{j,\lambda}e^{-ik_j z}\hat{v}_\lambda]. \tag{8}$$

Here, the real wave vector is $\vec{k}_j = (0, 0, k_j)$, with $k_j = n_j\omega/c$ and $n_j = \sqrt{\epsilon_j \mu_j}$ being the refraction index of the $j$th medium. $E_{j,\lambda}$ ($E'_{j,\lambda}$) is the amplitude of the wave traveling to the right (left). Also, $\hat{v}_\lambda = \hat{v}_\pm$ is given by

$$\hat{v}_\pm = \frac{1}{\sqrt{2}}\begin{pmatrix} 1 \\ \pm i \end{pmatrix}. \tag{9}$$

In addition, we have defined $g_{j,\lambda}$ as

$$g_{j,\lambda} = \frac{\alpha}{\mu_0 c\pi}\theta_j - \lambda\frac{i}{\omega\mu_0\mu_j}k_j, \tag{10}$$

with $\bar{g}_{j,\lambda}$ being the complex conjugate.

By starting from the interface, the boundary conditions are given by [51]

$$\vec{E}_{A,\lambda} = \vec{E}_{B,\lambda} \tag{11}$$

and

$$\vec{H}_{A,\lambda} = \vec{H}_{B,\lambda}. \tag{12}$$

Applying the above boundary conditions at $z = 0$ and using Eqs. (7) and (8), we have (one can omit the index $\lambda$ without loss of generality)

$$E_A + E'_A = E_B + E'_B \tag{13}$$

and

$$g_A E_A + \bar{g}_A E'_A = g_B E_B + \bar{g}_B E'_B. \tag{14}$$

Here, $E_B$ and $E'_B$ can be related to $E_A$ and $E'_A$ by a $2 \times 2$ interface matrix from medium $A$ to $B$,

$$\begin{pmatrix} E_B \\ E'_B \end{pmatrix} = M_{AB}\begin{pmatrix} E_A \\ E'_A \end{pmatrix}, \tag{15}$$

where

$$M_{AB} = \frac{1}{2i\Im[g_B]}\begin{pmatrix} g_A - \bar{g}_B & \bar{g}_A - \bar{g}_B \\ -g_A + g_B & -\bar{g}_A + \bar{g}_B \end{pmatrix}. \tag{16}$$

From Eqs. (13) and (14), one can obtain the $2 \times 2$ interface matrix $M_{BA}$ which relates the coefficients from medium $B$ to medium $A$,

$$\begin{pmatrix} E_A \\ E'_A \end{pmatrix} = M_{BA}\begin{pmatrix} E_B \\ E'_B \end{pmatrix}, \tag{17}$$

with

$$M_{BA} = \frac{1}{2i\text{Im}[g_A]}\begin{pmatrix} g_B - \bar{g}_A & \bar{g}_B - \bar{g}_A \\ -g_B + g_A & -\bar{g}_B + \bar{g}_A \end{pmatrix}. \tag{18}$$

A general expression for the transmission matrix, which connects the fields across an interface from medium $m$ to medium $n$, can be written as

$$M_{mn} = \frac{1}{2i\text{Im}[g_n]}\begin{pmatrix} g_m - \bar{g}_n & \bar{g}_m - \bar{g}_n \\ -g_m + g_n & -\bar{g}_m + \bar{g}_n \end{pmatrix}. \tag{19}$$

Here, $\text{Im}[g_n]$ corresponds to the imaginary part of $g$ for medium $n$, which is defined in Eq. (10). Finally, for the case of an electromagnetic wave propagating inside medium $j = A$ or $B$, with thickness $d_j$ and wave vector $k_j$, the $2 \times 2$ propagation matrix is given by

$$M_j = \begin{pmatrix} e^{ik_j d_j} & 0 \\ 0 & e^{-ik_j d_j} \end{pmatrix}. \tag{20}$$

See Ref. [52] for more details.

## B. Dispersion relation

In 1D photonic crystals composed of dielectric layers (or building blocks) arranged in a periodic fashion, the propagating electromagnetic waves are modulated by Bragg's scatterings, resulting in the photonic band structure, in which the photonic band gaps emerge. Consider the $l$th unit cell $[A|B]$ of a 1D APC. The electric fields inside layers $A$ and $B$ are labeled $\vec{E}_{A,l} = (E_{A,l}, E'_{A,l})$ and $\vec{E}_{B,l} = (E_{B,l}, E'_{B,l})$. In order to obtain the transfer matrix for this unit cell, one must relate the electric field coefficients of the $(l + 1)$th unit cell to the electric field coefficients of the $l$th unit cell. We can write for an electromagnetic wave, propagating from layer $A$ and crossing the interface from $A$ to $B$, both in the same $l$th unit cell,

$$\begin{pmatrix} E_{B,l} \\ E'_{B,l} \end{pmatrix} = M_A M_{AB}\begin{pmatrix} E_{A,l} \\ E'_{A,l} \end{pmatrix}. \tag{21}$$

In a similar way, we consider the electromagnetic wave propagating from layer $B$ and crossing the interface from $B$ to $A$, but now $B$ belongs to the $l$th unit cell, while $A$ belongs to the $(l + 1)$th unit cell,

$$\begin{pmatrix} E_{A,l+1} \\ E'_{A,l+1} \end{pmatrix} = M_B M_{BA}\begin{pmatrix} E_{B,l} \\ E'_{B,l} \end{pmatrix}. \tag{22}$$

By substituting Eq. (21) into Eq. (22), we get

$$\begin{pmatrix} E_{A,l+1} \\ E'_{A,l+1} \end{pmatrix} = M\begin{pmatrix} E_{A,l} \\ E'_{A,l} \end{pmatrix}, \tag{23}$$

where

$$M = M_B M_{BA} M_A M_{AB} \tag{24}$$

is the $2 \times 2$ transfer matrix for the whole unit cell $[A|B]$.

From Bloch's theorem, the eigenvalues of $M$ are related to Bloch's phase $QD$, which is the phase change in the fields after propagating along the unit cell. Here, $Q$ is Bloch's wave vector, and $D$ is the unit-cell size of the structure ($D = d_A + d_B$ in the present case). Therefore, Eq. (23) can be rewritten as

$$\begin{pmatrix} E_{A,l+1} \\ E'_{A,l+1} \end{pmatrix} = e^{iQD}\begin{pmatrix} E_{A,l} \\ E'_{A,l} \end{pmatrix} = M\begin{pmatrix} E_{A,l} \\ E'_{A,l} \end{pmatrix}. \tag{25}$$

On the other hand, for a wave propagating from the right to the left, Eq. (25) becomes

$$\begin{pmatrix} E_{A,l-1} \\ E'_{A,l-1} \end{pmatrix} = e^{-iQD}\begin{pmatrix} E_{A,l} \\ E'_{A,l} \end{pmatrix} = M^{-1}\begin{pmatrix} E_{A,l} \\ E'_{A,l} \end{pmatrix}. \tag{26}$$

Equations (25) and (26) may be also written as

$$[M - e^{iQD}\mathbb{1}]\begin{pmatrix} E_{A,l} \\ E'_{A,l} \end{pmatrix} = \begin{pmatrix} 0 \\ 0 \end{pmatrix} \tag{27}$$

and

$$[M^{-1} - e^{-iQD}\mathbb{1}]\begin{pmatrix} E_{A,l} \\ E'_{A,l} \end{pmatrix} = \begin{pmatrix} 0 \\ 0 \end{pmatrix}. \tag{28}$$

Here, $\mathbb{1}$ is the $2 \times 2$ identity matrix, and $M^{-1}$ is the inverse of the transfer matrix $M$. If we add Eqs. (27) and (28), we obtain

$$[M + M^{-1} - (e^{iQD} + e^{-iQD})\mathbb{1}]\begin{pmatrix} E_{A,l} \\ E'_{A,l} \end{pmatrix} = \begin{pmatrix} 0 \\ 0 \end{pmatrix}, \tag{29}$$

whose nontrivial solutions are obtained from the condition

$$\det[M + M^{-1} - (e^{iQD} + e^{-iQD})\mathbb{1}] = 0. \quad (30)$$

By using the fact that the transfer matrix is a unimodular matrix, i.e., its determinant $\det[M] = 1$, we can write Eq. (30) as an algebraic expression, i.e. [49],

$$\cos(QD) = \left(\frac{1}{2}\right)\mathrm{Tr}[M] = \frac{M_{11} + M_{22}}{2}. \quad (31)$$

Here, $\mathrm{Tr}[M]$ is the trace of the transfer matrix $M$, and $M_{11}$ and $M_{22}$ are their diagonal elements. Equation (31) is a transcendental equation, and it shows that, since we are able to obtain the transfer matrix $M$ of the system, we can numerically obtain its solutions; that is, we can obtain the frequencies for which Bloch's wave vector $Q$ is real. The allowed frequencies are such that the condition $|(1/2)\mathrm{Tr}[M]| \leqslant 1$ is satisfied. Otherwise, if $|(1/2)\mathrm{Tr}[M]| > 1$, Bloch's wave vector is complex, and consequently, the light wave has an evanescent profile, and the photonic band gaps emerge. For an allowed band, from Eq. (31) we obtain

$$Q = \frac{\cos^{-1}[(M_{11} + M_{22})/2]}{D}, \quad (32)$$

so that Bloch's wave vector $Q$ varies from $-\pi/D$ to $\pi/D$, which is the unit-cell size in reciprocal space.

In our case of interest, a 1D APC composed of two building blocks, $A$ and $B$, with dielectric permittivities $\epsilon_j$, magnetic permeabilities $\mu_j$, topological parameters $\theta_j$, and thickness $d_j$ ($j = A$ or $B$) whose unit cell $[A|B]$ is arranged in a periodic fashion, Eq. (31), can be analytically obtained (see Ref. [49] for more details),

$$\cos(QD) = \cos(\phi_A)\cos(\phi_B) - \Delta \sin(\phi_A)\sin(\phi_B), \quad (33)$$

with $\phi_j = k_j d_j$ being the phase of medium $j$ and

$$\Delta = \frac{1}{2}\left\{\frac{k_B \mu_A}{k_A \mu_B} + \frac{k_A \mu_B}{k_B \mu_A} + \left[\frac{\omega\alpha(\theta_A - \theta_B)}{c\pi}\right]^2 \frac{\mu_A \mu_B}{k_A k_B}\right\}$$
$$= \frac{1}{2}\left\{\frac{Z_A}{Z_B} + \frac{Z_B}{Z_A} + \delta Z_A Z_B\right\}. \quad (34)$$

Here, $Z_j = \sqrt{\mu_j/\epsilon_j}$ is the impedance of medium $j$, and

$$\delta = \left[\frac{\pi(\theta_A - \theta_B)}{\alpha}\right]^2. \quad (35)$$

The first two terms in Eq. (34) are responsible for the emergence of the conventional photonic band gaps, whose physical origin relies on Bragg's scattering. The third term in Eq. (34), containing the topological parameters, is responsible for the emergence of non-Bragg's photonic band gaps. As expected, by taking the limit $\delta \to 0$, Eq. (34) reduces to the dispersion relation of a conventional (nonaxionic) 1D PC [49]. Also, notice that $\delta = 0$ only for $\theta_A = \theta_B \neq 0$ or $\theta_A = \theta_B = 0$. This means that, even for $\epsilon_A = \epsilon_B$ and $\mu_A = \mu_B$, a photonic band gap will be expected to emerge for any values of $\theta_A$ and $\theta_B$ with $\theta_A \neq \theta_B$.

## III. NUMERICAL RESULTS

In this section we present the numerical results for the band structures for normally incident electromagnetic waves in 1D
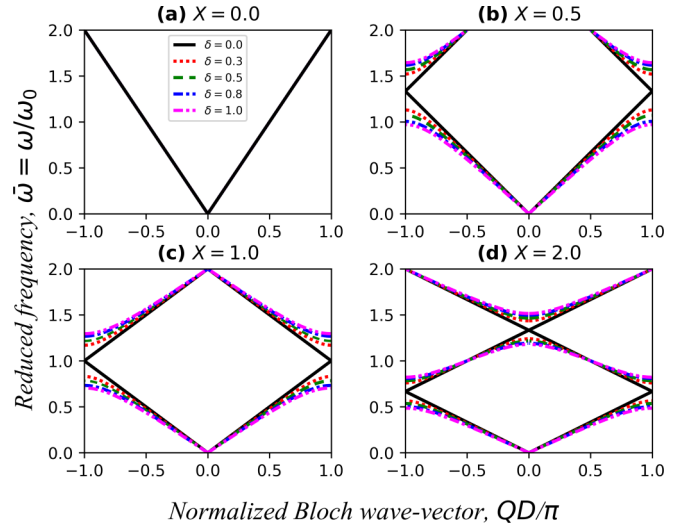


FIG. 2. Band structure of the axionic photonic crystal, considering $R = 1.0$, with (a) $X = 0.0$, (b) $X = 0.5$, (c) $X = 1.0$, and (d) $X = 2.0$. The different values of $\delta$ are indicated.

APCs. From now on, we assume that the axionic photonic crystal consists of two alternating building blocks, represented by $A$ and $B$, and both are nonmagnetic materials, i.e., $\mu_A = \mu_B = 1$. Also, according to Eq. (35), the topological parameters are related by $\theta_B = \theta_A - \pi\sqrt{\delta}/\alpha$ [53]. For the central wavelength $\lambda_0$, we have defined a midgap frequency $\omega_0 = 2\pi c/\lambda_0 = 10^{12}$ rad/s. Thus, the band structures are all given in terms of the dimensionless reduced frequency $\bar{\omega} = \omega/\omega_0$ and the normalized Bloch's wave vector $QD/\pi$. In this paper we defined the thickness of layer $A$ as $d_A = \lambda_0/4n_A$, satisfying the quarter-wavelength condition; that is, the thickness of layer $A$ is defined as being a quarter of the central wavelength [49]. The thickness of layer $B$ is obtained from the values of $X$.

Let us consider the most trivial case. We calculated the band structure of a 1D APC with $R = \epsilon_B/\epsilon_A = 1$ for different values of $X = d_B/d_A$ and $\delta$ in order to infer the effects of the topological parameters on the light dispersion relation. We should remark that this is not a realistic situation. However, it can provide us valuable insights about different axionic photonic materials presenting similar dielectric constants, i.e., materials that present $\epsilon_A \approx \epsilon_B$. The band structures are plotted in Figs. 2(a)–2(d) for $X = 0.0$, $X = 0.5$, $X = 1.0$, and $X = 2.0$, respectively. The different values of $\delta$ are indicated in the legend of Fig. 2, and a given curve corresponds to a specific value of $\delta$. As expected, from Fig. 2, for $\delta = 0$ ($\theta_A = \theta_B$), the band structure has no gap, and the light is transmitted through the structure without any reflection, despite the values of $X$, corresponding to $\Delta = 1$ in Eq. (34). One can also observe from Fig. 2(a) that, no matter what the value of $\delta$ is, there is no band gap. This is because the system is a continuous medium without interfaces ($X = 0.0$). However, for $X \neq 0$ and $\delta \neq 0$, we can observe that a range of forbidden frequencies naturally emerges in Figs. 2(b), 2(c), and 2(d). Those photonic band gaps provide us the means of controlling the propagation of light by manipulating the topological parameters of the system. We can also observe that, for a given value of $X$, the
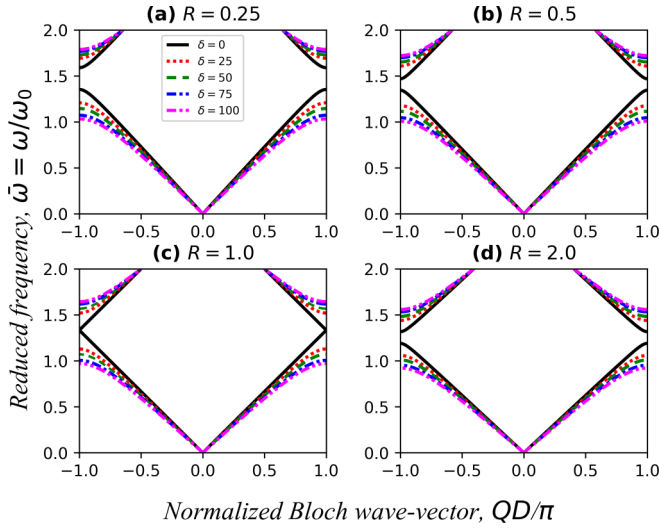
FIG. 3. Same as Fig. 2, considering $X = 0.5$, with (a) $R = 0.25$, (b) $R = 0.5$, (c) $R = 1.0$, and (d) $R = 2.0$. The different values of $\delta$ are indicated.



FIG. 5. Same as Fig. 3, but for $X = 2.0$.

band-gap width becomes wider as the $\delta$ parameter increases, although the band-gap center appears not to be considerably affected. On the other hand, the band-gap centers are shifted to the low-frequency regions, and also, the band gaps become narrower as the ratio of the thicknesses $X$ is increased [since $X \neq 0$; see Figs. 2(b)–(d)]. This behavior also occurs in conventional photonic crystals [54].

Let us now consider a more realistic situation: a structure in which the two building blocks present different dielectric permittivities, i.e., $\epsilon_A \neq \epsilon_B$. We consider $X = 0.5$, $1.0$, and $2.0$, and the corresponding photonic band structures are presented in Figs. 3–5, respectively, with $R = 0.25$, $R = 0.5$, $R = 1.0$, and $R = 2.0$. We can notice from Figs. 3–5 that the band structures are very similar to those of Fig. 2. However, now the band gaps have two contributions: Bragg's scattering and the topological term [see Eq. (34) and the discussion about it].
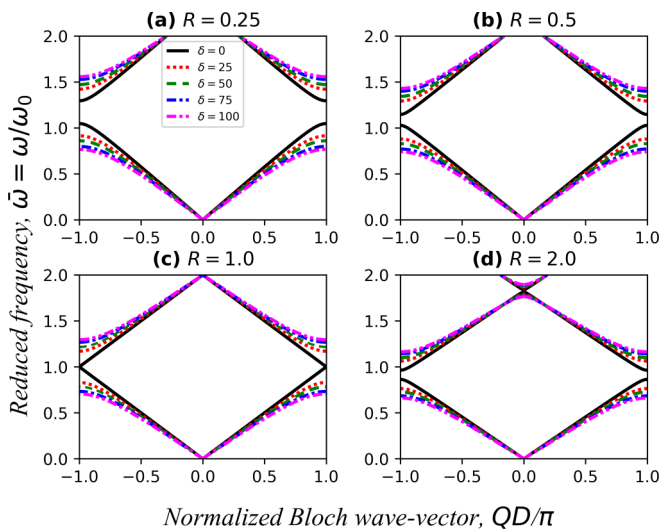
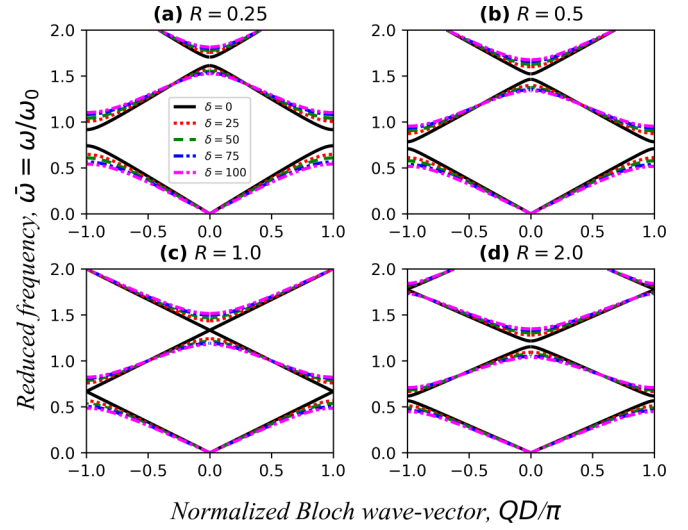Figure 3, with $X = 0.5$, shows that the lower edge of the gap is around $\bar{\omega} \approx 1.1$. For a given $\delta$, the position of the center of the band gap is shifted to lower-frequency regions as $R$ increases. On the other hand, for a given $R$, the band gaps' width becomes wider as the topological parameter $\delta$ increases, while the band gaps' center is not substantially affected. Moreover, we can see that the upper edge is less shifted than the lower edge; that is, the upper and lower edges of the band gap are slightly asymmetrically shifted to higher and lower frequencies, respectively. We can infer that the band gaps are very sensitive to the difference between the topological parameters $\theta_A$ and $\theta_B$ at the interfaces. In Figs. 4 and 5 we present plots which are qualitatively analogous to the plots of Fig. 3, but with slight differences. For example, the position of the center of the band gap is around $\bar{\omega} \approx 1.0$ in Fig. 4 and $\bar{\omega} \leqslant 1.0$ in Fig. 5. All other features of the band
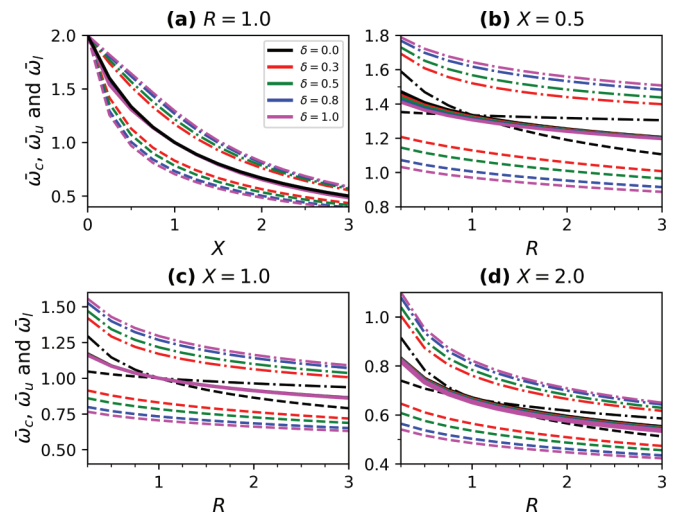


FIG. 4. Same as Fig. 3, but for $X = 1.0$.



FIG. 6. Plots of $\bar{\omega}_c$ (solid lines), $\bar{\omega}_u$ (dot-dashed lines), and $\bar{\omega}_l$ (dashed lines) as a function of (a) $X$, considering $R = 1.0$, and of $R$ for (b) $X = 0.5$, (c) $X = 1.0$, and (d) $X = 2.0$.
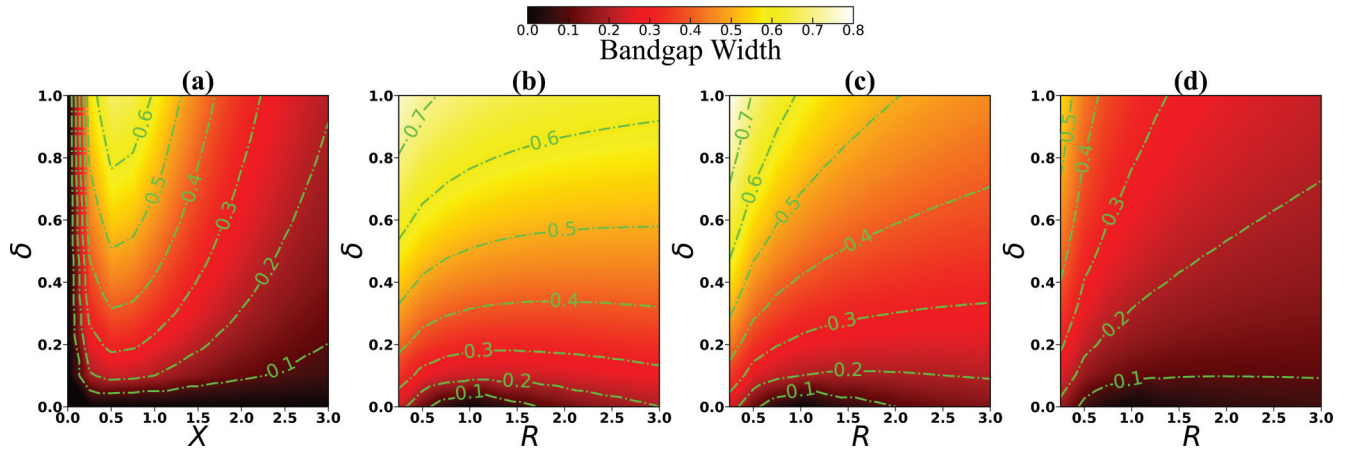
FIG. 7. Surface plots of the band-gap widths as a function of (a) $\delta$ and $X$, considering $R = 1.0$, and of $\delta$ and $R$ for (b) $X = 0.5$, (c) $X = 1.0$, and (d) $X = 2.0$.

structure related to $R$ and $\delta$ are qualitatively the same as in Fig. 3.

For technological applications it is quite relevant to know how the band structure is affected by the physical $R$, geometrical $X$, and topological $\delta$ parameters. More specifically, we are interested in the center and edge positions, as well as the width, of the first band gap. Let us illustrate our numerical results in Figs. 6 and 7. In Fig. 6 we present the plots of the reduced frequencies corresponding to the center $\bar{\omega}_c$, upper edge $\bar{\omega}_u$, and lower edge $\bar{\omega}_l$ of the first band gap for different values of $\delta$. Those frequencies are represented by the solid, dot-dashed, and dashed lines, respectively. Figure 6(a) shows $\bar{\omega}_c$, $\bar{\omega}_u$, and $\bar{\omega}_l$ as a function of $X$ with $R = 1.0$. In agreement with Fig. 2, the band gap is null for $\delta = 0$. As we can also see, the center of the band gap is not really affected by $\delta$, while the band gap width reaches its maximum around $X \approx 1.0$. In Figs. 6(b)–6(d), we present the same plot as in Fig. 6(a), but now with $\bar{\omega}_c$, $\bar{\omega}_u$, and $\bar{\omega}_l$ as a function of $R$ for $X = 0.5$, $X = 1.0$, and $X = 2.0$, respectively. As observed in Figs. 2–5, the gaps are non-null once the condition $R \neq 1.0$ and $\delta \neq 0$ is satisfied. The topological effects on the photonic band structures are now clearer and more evident. From Figs. 6(b)–6(d), considering $\delta = 0$ (corresponding to a conventional photonic crystal), for $0 < R < 1$, the band gap becomes narrower until it vanishes when $R = 1.0$. On the other hand, for $R > 1$, the band gap is not null anymore, and it becomes wider as $R$ increases. In addition, we can observe that the superior and inferior edges of the band gap are slightly asymmetrical; that is, they have approximately the same relative distance from the center of the gap. However, for $\delta \neq 0$, the band gap does not vanish even for $R = 1.0$. The center of the band gap presents the same behavior as in the $\delta = 0$ case. For a given value of $R$, the band-gap width becomes monotonically wider as $\delta$ increases, while for a given $\delta$ (since $\delta \neq 0$), the band-gap width becomes narrower as $R$ becomes higher. It is interesting that the band-gap width for the conventional photonic crystal works as the limit case; that is, the band-gap width for $\delta \neq 0$ cannot be narrower than that for $\delta = 0$. From the results presented up to now, one can conclude that we have several ways to combine the geometrical $X$, physical $R$, and topological $\delta$ parameters to manipulate the edges and center of the band

gap to control light wave propagation in 1D APCs. Thus, for the purpose of knowing which set of parameters provides the wider band gap, we show the band-gap width as a function of $\delta$ and $X$ and $\delta$ and $R$ in Fig. 7. Figure 7(a) shows the surface plot of the width of the first band gap as a function of $\delta$ and $X$, with $R = 1.0$, while Figs. 7(b)–7(d) show the surface plot of the width of the first band gap as a function of $\delta$ and $R$ for $X = 0.5$, $X = 1.0$, and $X = 2.0$, respectively. In Fig. 7 the color scale indicates band-gap width from 0 (black) and to 0.8 (white). Also, the green dot-dashed lines represent the level curves for some values of the band-gap width.

Figure 7(a) confirms that the band gap is null for any value of $X$ when $\delta = 0$ and for any value of $\delta$ when $X = 0.0$. We can observe from Figs. 7(b)–7(d) that the band-gap width vanishes whenever $\delta = 0$ and $R = 1.0$ (dark regions). On the other hand, the wider band gaps (larger than 0.6 and represented by the brighter regions) are obtained for (i) $\delta > 0.8$, $X \approx 0.5$, and $R = 1.0$ in Fig. 7(a); (ii) $\delta > 0.6$, $R \approx 0.25$, and $X = 0.5$ in Fig. 7(b); and (iii) $\delta > 0.5$, $R \approx 0.25$, and $X = 1.0$ in Fig. 7(c). There is no band gap larger than 0.6 in Fig. 7(d). Therefore, from Fig. 7 one can conclude that the topological parameter $\delta$ works almost independently of the geometrical $X$ and physical $R$ parameters; that is, the band-gap width is always wider if $\delta$ increases, no matter the values of $X$ and $R$ are. On the contrary, $X$ and $R$ work against each other; that is, as $X$ increases, $R$ must decrease for a wide band-gap emergence and vice versa.

## IV. CONCLUSIONS

In summary, we have used a transfer matrix method to study the propagation of circularly polarized light waves in an axionic layered medium. We calculated the dispersion spectra to investigate the structure of band gaps of this material. We presented numerical results for the photonic band structure as a function of the ratio between permittivities $R = \epsilon_B/\epsilon_A$, layer thicknesses $X = d_B/d_A$, and topological parameters $\delta = \pi^2(\theta_A - \theta_B)^2/\alpha^2$. We found that, for a given value of $X$ (since $X \neq 0$), the band-gap width becomes wider as the $\delta$ parameter increases, although the band-gap center appear not to be considerably affected. On the one hand, the band-gap centers are

shifted to the low-frequency regions, and also, the band gaps become narrower as the ratio between the thicknesses $X$ is increased. Also, for a given $\delta$, the position of the center of the band gap is shifted to lower-frequency regions as $R$ increases. On the other hand, for a given $R$, the band-gap width becomes wider as the topological parameter $\delta$ increases, but the band-gap center is not affected. It was also observed that the band-gap upper edge is less shifted than the band-gap lower edge; that is, the upper and lower edges of the band gap are slightly asymmetrically shifted. On the one hand, considering $\delta = 0$ (corresponding to a conventional photonic crystal), for $0 < R < 1$, the band gap becomes narrower until it vanishes when $R = 1.0$. On the other hand, for $R > 1$, the band gap is not null anymore, and it becomes wider as $R$ increases. However, for $\delta \neq 0$ (corresponding to an axionic photonic crystal), the band gap does not vanish even for $R = 1.0$. For a given value of $R$, the band-gap width becomes monotonically wider as $\delta$ increases, while for a given $\delta$, the band-gap width becomes narrower as $R$ becomes higher. One can conclude that the topological parameter $\delta$ works almost independently of the geometrical $X$ and physical $R$ parameters; that is, the band-gap width is always wider if $\delta$ increases no matter what the values of $X$ and $R$ are. On the other hand, $X$ and $R$ work against each other; that is, as $X$ increases, $R$ must decrease for a wide band-gap emergence and vice versa. Our results open possibilities for technological applications of axionic photonic crystals by manipulating the flow of light by means of the topological parameter of the system. Surely, our model can be realized experimentally, and we hope that experimentalists are encouraged to face it.

### ACKNOWLEDGMENTS

[1] Lord Rayleigh, London, Edinburgh Dublin Philos. Mag. J. Sci. **24**, 145 (1887).

[2] E. Yablonovitch, Phys. Rev. Lett. **58**, 2059 (1987).

[3] S. John, Phys. Rev. Lett. **58**, 2486 (1987).

[4] M. Notomi, Rep. Prog. Phys. **73**, 096501 (2010).

[5] K. M. Ho, C. T. Chan, and C. M. Soukoulis, Phys. Rev. Lett. **65**, 3152 (1990).

[6] *Photonic Band Gap Materials*, edited by C. M. Soukoulis, NATO ASI Series (Springer, Berlin, 2012), Vol. 315.

[7] M. Johri, Y. Ahmed, and T. Bezboruah, Curr. Sci. **92**, 1361 (2007).

[8] C. L. Kane and E. J. Mele, Phys. Rev. Lett. **95**, 146802 (2005).

[9] J. E. Moore, Nature (London) **464**, 194 (2010).

[10] L. Fu, Phys. Rev. Lett. **106**, 106802 (2011).

[11] N. Varnava and D. Vanderbilt, Phys. Rev. B **98**, 245117 (2018).

[12] F. Schindler, A. M. Cook, M. G. Vergniory, Z. Wang, S. S. Parkin, B. A. Bernevig, and T. Neupert, Sci. Adv. **4**, eaat0346 (2018).

[13] Y. Tanaka, Z. Ren, T. Sato, K. Nakayama, S. Souma, T. Takahashi, K. Segawa, and Y. Ando, Nat. Phys. **8**, 800 (2012).

[14] M. Konig, S. Wiedmann, C. Brune, A. Roth, H. Buhmann, L. W. Molenkamp, X.-L. Qi, and S.-C. Zhang, Science **318**, 766 (2007).

[15] Y. Chen, J. G. Analytis, J.-H. Chu, Z. Liu, S.-K. Mo, X.- L. Qi, H. Zhang, D. Lu, X. Dai, Z. Fang, S. C. Zhang, I. R. Fisher, Z. Hussain, and Z.-X. Shen, Science **325**, 178 (2009).

[16] M. Z. Hasan and C. L. Kane, Rev. Mod. Phys. **82**, 3045 (2010).

[17] W. Tian, W. Yu, J. Shi, and Y. Wang, Materials **10**, 814 (2017).

[18] Y. Yang, Z. Gao, H. Xue, L. Zhang, M. He, Z. Yang, R. Singh, Y. Chong, B. Zhang, and H. Chen, Nature (London) **565**, 622 (2019).

[19] M. A. Bandres, S. Wittek, G. Harari, M. Parto, J. Ren, M. Segev, D. N. Christodoulides, and M. Khajavikhan, Science **359**, eaar4005 (2018).

[20] G. Harari, M. A. Bandres, Y. Lumer, M. C. Rechtsman, Y. D. Chong, M. Khajavikhan, D. N. Christodoulides, and M. Segev, Science **359**, eaar4003 (2018).

[21] J. Zhang, C.-Z. Chang, Z. Zhang, J. Wen, X. Feng, K. Li, M. Liu, K. He, L. Wang, X. Chen, Q. K. Xue, X. Ma, and Y. Wang, Nat. Commun. **2**, 574 (2011).

[22] A. M. Essin, J. E. Moore, and D. Vanderbilt, Phys. Rev. Lett. **102**, 146805 (2009).

[23] R. D. Peccei and H. R. Quinn, Phys. Rev. Lett. **38**, 1440 (1977).

[24] F. W. Hehl, Y. N. Obukhov, J.-P. Rivera, and H. Schmid, Phys. Lett. A **372**, 1141 (2008).

[25] F. W. Hehl, Y. N. Obukhov, J.-P. Rivera, and H. Schmid, Eur. Phys. J. B **71**, 321 (2009).

[26] E. Kita, K. Siratori, and A. Tasaki, J. Appl. Phys. **50**, 7748 (1979).

[27] A. Sekine and K. Nomura, J. Appl. Phys. **129**, 141101 (2021)

[28] A. Martin-Ruiz, O. Rodriguez-Tzompantzi, J. R. Maze, and L. F. Urrutia, Phys. Rev. A **100**, 042124 (2019).

[29] M. Mogi, M. Kawamura, A. Tsukazaki, R. Yoshimi, K. S. Takahashi, M. Kawasaki, and Y. Tokura, Sci. Adv. **3**, eaao1669 (2017).

[30] L. Visinelli, Mod. Phys. Lett. A **28**, 1350162 (2014).

[31] T. Morimoto, A. Furusaki, and N. Nagaosa, Phys. Rev. B **92**, 085113 (2015).

[32] N. P. Armitage and L. Wu, SciPost Phys. **6**, 046 (2019).

[33] S. Ozaki and N. Yamamoto, J. High Energy Phys. 08 (2017) 098.

[34] E. J. C. Granada and D. F. Rojas, J. Phys.: Conf. Ser. **850**, 012024 (2017).

[35] S. Raghu and F. D. M. Haldane, Phys. Rev. A **78**, 033834 (2008).

[36] M. C. Rechtsman, J. M. Zeuner, Y. Plotnik, Y. Lumer, D. Podolsky, F. Dreisow, S. Nolte, M. Segev, and A. Szameit, Nature (London) **496**, 196 (2013).

[37] L. Lu, J. Joannopoulos, and M. J. Soljačić, Nat. Photonics **8**, 821 (2014).

[38] T. Ozawa, H. M. Price, A. Amo, N. Goldman, M. Hafezi, L. Lu, M. C. Rechtsman, D. Schuster, J. Simon, O. Zilberberg, and I. Carusotto, Rev. Mod. Phys. **91**, 015006 (2019).

[39] F. D. M. Haldane and S. Raghu, Phys. Rev. Lett. **100**, 013904 (2008).

[40] A. B. Khanikaev and G. Shvets, Nat. Photonics **11**, 763 (2017).

[41] G. Siroki, P. A. Huidobro, and V. Giannini, Phys. Rev. B **96**, 041408(R) (2017).

[42] M. Kim, Z. Jacob, and J. Rho, Light: Sci. Appl. **9**, 130 (2020).

[43] N. Parappurath, F. Alpeggiani, L. Kuipers, and E. Verhagen, Sci. Adv. **6**, eaaw4137 (2020).

[44] Z. Zhang, M. H. Teimourpour, J. Arkinstall, M. Pan, P. Miao, H. Schomerus, R. El-Ganainy, and L. Feng, Laser Photonics Rev. **13**, 1800202 (2019).

[45] I. V. Lindell, A. H. Sihvola, S. A. Tretyakov, A. J. Viitanen, *Electromagnetic Waves in Chiral and Bi-Isotropic Media* (Artech House, Boston, 1994).

[46] J. C. G. Henriques, T. G. Rappoport, Y. V. Bludov, M. I. Vasilevskiy, and N. M. R. Peres, Phys. Rev. A **101**, 043811 (2020).

[47] A. B. Khanikaev, S. Hossein Mousavi, W.-K. Tse, M. Kargarian, A. H. MacDonald, and G. Shvets, Nat. Mater. **12**, 233 (2013).

[48] S. Barik, A. Karasahin, C. Flower, T. Cai, H. Miyake, W. DeGottardi, M. Hafezi, and E. Waks, Science **359**, 666 (2018).

[49] P. Markos and C. M. Soukoulis, *Wave Propagation: From Electrons to Photonic Crystals and Left-Handed Materials* (Princeton University Press, Princeton, NJ, 2008).

[50] A. Karch, Phys. Rev. B **83**, 245432 (2011)

[51] D. J. Griffiths, *Introduction to electrodynamics* (Cambridge University Press, New York, 2005).

[52] C. H. Costa, L. F. C. Pereira, and C. G. Bezerra, Phys. Rev. B **96**, 125412 (2017).

[53] M. Vieira, S. Sergeenkov, and C. Furtado, Phys. Rev. A **96**, 013852 (2017).

[54] B. P. Silva and C. H. Costa, J. Phys.: Condens. Matter **32**, 135703 (2019).